Modeling and Transceiver Design for Asymmetric UWB Links with Heterogeneous Nodes

Huilin Xu, *Student Member, IEEE,* and Liuqing Yang, *Senior Member, IEEE*

***Abstract*—In recent years, Ultra-Wideband (UWB) technology has emerged as a promising physical layer candidate for a wide range of wireless networks, especially due to its low operation power level and coexistence ability with traditional wireless systems. However, none of these physical layer realizations has specified the compatible operation among them (see, e.g., [1], [15], [24]). Therefore, the effective interoperability between asymmetric UWB transceivers needs to be considered for ubiquitous wireless communications. In this paper, we investigate the transceiver design for asymmetric UWB links with a single transmitter and a single receiver. We consider factors that can lead to the asymmetry between UWB transmitters and receivers such as different numbers of signal bands and different pulse rates. Our analysis reveals the similarity between the asymmetric UWB links and the conventional multiantenna systems. Then, MIMO signal processing approaches can be readily applied to achieve the optimal design in terms of channel throughput or bit error rate (BER). Analysis and simulations corroborate the effectiveness of our transceiver designs.**

***Index Terms*—Ultra-Wideband (UWB), multi-input multi-output (MIMO), asymmetric link, multiband system.**

I. Introduction

In recent years, Ultra-Wideband (UWB) technology has attracted increasing interests for its coexistence with current wireless systems by accessing the unlicensed spectrum at an extremely low power level. The huge bandwidth of UWB can guarantee a large channel capacity without invoking high transmit power. Due to these unique features, UWB has been proposed as the physical layer realization for various networks, including both the high data rate[1] and low data rate wireless personal area networks (WPANs) (see, e.g., [1], [9], [24]), the wireless body area networks (WBANs) (see, e.g., [15]) and the wireless sensor networks (WSNs) (see, e.g., [21], [36]). As these systems can provide various services, heterogeneity emerges among network nodes either inside a network or among different ones. To realize the seamless network operation, transceiver design needs to take into account the heterogeneity among these nodes.

Paper approved by S. N. Batalama, the Editor for Spread Spectrum and Estimation of the IEEE Communications Society. Manuscript received June 27, 2007; revised May 27, 2008 and December 4, 2008.

The authors are with the Department of Electrical and Computer Engineering, University of Florida, P.O. Box 116130, Gainesville, FL 32611, USA (e-mail: xuhl@ufl.edu, lqyang@ece.ufl.edu).

Part of the results in this paper has been presented at the IEEE International Workshop on Signal Processing Advances in Wireless Communications, 2005, and the IEEE International Conference on Communications, 2008. This work was supported by the National Science Foundation under Grant ECS-0621879.

Digital Object Identifier 10.1109/TCOMM.2010.06.070276

[1]IEEE 802.15.3a Task Group was officially disbanded in 2006, but the products are still being made in the industry.

Heterogeneity has been investigated for the higher layer issues including scheduling, polling and routing, etc., for the UWB-based or general wireless networks (see, e.g., [3], [17], [37]). In this paper, we focus on the physical layer heterogeneity of the asymmetric UWB links. For UWB links, heterogeneity and asymmetry can be induced by the different numbers of signal bands for multiband operation, different pulse rates or different pulse shapers, between the transmitter and the receiver. Here, we are more interested in the first two factors, i.e., the number of signal bands and the pulse rate, because these factors usually determine the complexity of the device. Generally, nodes of high complexity can provide high data rate services such as the multimedia data transfer which needs more power and computational resources. Nodes of low complexity are typically small and rely on limited battery power, such as wireless sensors. Besides these, some researchers have also considered the complexity-performance tradeoff of UWB transceivers by choosing different ADC resolutions (see e.g., [4], [12], [28]). However, since the ADC resolution does not affect our system modeling and the transceiver design, here we will not discuss this issue.

In this paper, we investigate the transceiver design for the asymmetric UWB link with a single transmitter and a single receiver. We first introduce the general transceiver model that allows for the information exchange on multiple bands at variable pulse repetition rates. By varying the band number or the pulse rate, the complexity level and accordingly the data rate of the link can be changed. Analyzing this mathematical model, we find that the asymmetric link can be represented by a multi-input multi-output (MIMO) system model which has originally been proposed and investigated for the multiple Tx- and Rx-antenna systems. The similarity between the asymmetric links and the multiantenna systems reveals that the structure asymmetry of these UWB transceivers is essentially equivalent to the spatial asymmetry of multiantenna systems. As far as we know, we are among the first to observe and exploit the similarity between these two types of asymmetric systems (see, e.g., [33], [35]).

Once the asymmetric UWB link is modeled as a MIMO system, we can apply existing multiantenna communication techniques to our UWB transceiver design for better performance or lower complexity. This is very attractive since many multiantenna techniques are available in the literature which are optimal in terms of system throughput, error rate or complexity, etc (see, e.g., [22], [25], [26], [34]). Then, we will show how these techniques can be integrated into our asymmetric link model. It should be noted that the MIMO modeling actually allows us to exploit the multipath diversity

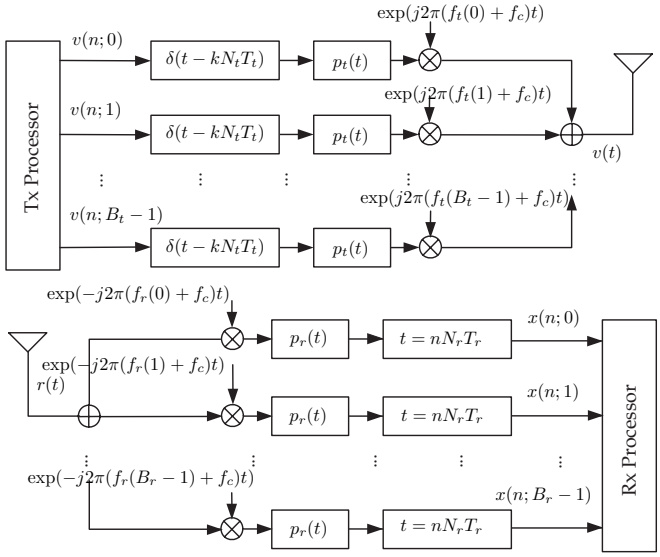

Fig. 1. UWB transmitter and receiver diagrams.

of the UWB channel in very flexible manners. In addition, by changing the parameters of our design, the MIMO modeling also enables the convenient rate-diversity tradeoff. Our analyses, together with the simulations, confirm the feasibility and effectiveness of the modeling and transceiver design for the asymmetric UWB link.

Notation: gcd{} denotes the greatest common divisor of integers; $\lceil\cdot\rceil$ and $\lfloor\cdot\rfloor$ stand for integer ceiling and floor operations, respectively; $\otimes$ denotes the Kronecker product; we use boldface upper/lower-case letters for matrices/vectors; $\boldsymbol{I}_N$ denotes the $N\times N$ identity matrix, and $\boldsymbol{F}_N$ the $N\times N$ FFT matrix; $\boldsymbol{F}_{N,0:M}$ captures the first $(M+1)$ columns of $\boldsymbol{F}_N$; $(\cdot)^T$ and $(\cdot)^{\mathcal{H}}$ stand for transpose and Hermitian operations, respectively.

II. Transceiver Structures

Fig. 1 shows the UWB transmitter and receiver structures used in this paper. Note that our transceiver does not necessarily represent any specific one utilized by existing standards, but combines functions of an array of transceivers into one framework. Both the transmitter and receiver can incorporate multiband operation.

At the transmitter, B_t parallel data streams $\{v(n;b)\}_{b=0}^{B_t-1}$ are modulated on the unit-energy pulse shaper $p_t(t)$ with the duration of T_t, the bandwidth of which is approximately $1/T_t$. With a pulse rate of $1/(N_tT_t)$ and N_t being an integer, the B_t data modulated pulse trains are fanned out simultaneously on B_t bands $\{f_c+f_t(b)\}_{b=0}^{B_t-1}$, with f_c being the center frequency of the first signal band and $f_t(b)=b/T_t$, $b\in[0,B_t-1]$. The transmitted signal is then given by:

$$v(t)=\sum_{b=0}^{B_t-1}\sum_{n=0}^{\infty}v(n;b)p_t(t-nN_tT_t)\exp(j2\pi(f_c+f_t(b))t)\ . \tag{1}$$

At the receiver, the received waveform $r(t)$ is carrier demodulated into B_r signal bands by multiplying it with $e^{-j2\pi(f_c+f_r(b))t}$, $b\in[0,B_r-1]$, and then sampled by a correlator with the template $p_r(t)$ at intervals of N_rT_r, with the width of $p_r(t)$ being T_r and N_r being an integer. We can then obtain B_r discrete-time data streams $x(n;b)$, $b\in[0,B_r-1]$

$$x(n;b)=\int_{nN_rT_r}^{(nN_r+1)T_r} r(t)\exp(-j2\pi(f_c+f_r(b))t) \times p_r(t)dt\ ,b\in[0,B_r-1]\ , \tag{2}$$

where $f_r(b)=b/T_r$, $b\in[0,B_r-1]$. The receiver could be different from the transmitter in terms of the pulse width, pulse rate or band number, which will result in the asymmetry between the transmitter and the receiver.

The multiband operation at the receiver was actually inspired by the idea of the "channelized UWB receiver" (see, e.g., [7], [20], [31]). Since the bandwidth of UWB signals is very large, it is not desirable to sample the received signal at the Nyquist rate with a single ADC. In order to solve this problem, the channelized receiver analyzes the received waveform into several narrower subbands and samples each subband with a much lower rate ADC. Then, the multiple digital signal streams are synthesized in the digital domain to reconstruct the digitalized version of the original waveform. Similarly, the limited DAC rate could be a hurdle to the digital UWB transmitter when the signal bandwidth is huge. To address this problem, we propose to process the subband digital streams with low-rate DAC's and then synthesize the resultant subband waveforms in analog domain. In this sense, the proposed multiband transmitter can be regarded as the counterpart of the channelized receiver. By this means, the all-digital UWB receiver proposed in [19] can hopefully be realized at a relatively low complexity level.

At our receiver, mixers and correlator-based samplers act as the bandpass filter bank and the Nyquist rate samplers in the channelized UWB receiver. Unlike the channelized UWB receiver, the oversampling or Nyquist sampling is not required by our receiver. As a result, the complexity can be reduced by our receiver with acceptable performance loss (see, e.g., [11]). When $B_t>1$, our transmitter can be regarded as the channelized UWB transmitter. With the pulse rate of $1/(N_tT_t)$, the same information transmission rate can be achieved as the single-band UWB transmitter with a higher pulse rate $B/(N_tT_t)$. Notice that the drawback of multiband operation of both our transceiver and the channelized UWB receiver (see, e.g., [7], [20]) is that the frequency skew needs to be tracked and calibrated for all frequency generators.

III. Modeling of the Asymmetric UWB Link

In the preceding section, we have introduced the structure of the UWB transceiver that forms the asymmetric UWB link. Heterogeneity and asymmetry can emerge when the transmitter and the receiver have different system parameters, especially when one node uses multiple bands while the other one uses a single band. Generally, the multiple frequency generators of the multiband node requires higher hardware cost than the single-band node. Therefore, the single-band node is more suitable for the low-complexity and small-sized device, such as the wireless sensor. In the following part of this section, we will investigate the input-output (I/O) relationship of the asymmetric link and establish a feasible model for information transmission.

A. Multiband Transmitter and Single-Band Receiver

First, let us consider a scenario where the transmitter operates with $B_t > 1$ signal bands and pulse rate $1/(N_tT_t)$, and the receiver operates with a single band and pulse rate $1/(N_rT_r)$. As described in section II, the bandwidth occupied by the transmitted signal is approximately B_t/T_t, and the bandwidth captured by the receiver is approximately $1/T_r$. In order to access the same bandwidth at both the transmitter and the receiver, we require their pulse width to satisfy $T_t = B_tT_r$.

Given the channel impulse response (CIR) $h(t)$, the received waveform can be expressed as $r(t) = v(t) * h(t) + n(t)$, with $n(t)$ being the additive noise. Carrier demodulating $r(t)$ by multiplying it with $\exp(-\jmath 2\pi f_c t)$, we have

$$x(t) = \sum_{b=0}^{B_t-1}\sum_{n=0}^{\infty} v(n;b)\hat{p}(t - nN_tT_t; b) + \eta(t)\ , \qquad (3)$$

where $\hat{p}(t;b) = \exp(\jmath 2\pi f_t(b)t)\int p_t(t-\tau)\exp(-\jmath 2\pi(f_c + f_t(b))\tau)h(\tau)d\tau$ can be regarded as the equivalent pulse shaper on the bth band and $\eta(t)$ is the filtered noise. To establish Eq. (3), we used the fact that $\exp(\jmath 2\pi f_t(b)N_tT_t) = 1$. The continuous-time signal $x(t)$ is sampled by the correlator $p_r(t)$ at intervals of N_rT_r to generate the discrete-time sequence

$$x(k) = \sum_{b=0}^{B_t-1}\sum_{n=0}^{\infty} v(n;b)R_{t,r}(kN_rT_r - nN_tT_t; b) + \eta(k)\ , \quad (4)$$

where $R_{t,r}(t) = \int \hat{p}_t(t+\tau)p_r(\tau)d\tau$.

In Eq. (4), the signal sequence $x(k)$ is the superposition of B_t data streams riding on the B_t signal bands. However, even for each band, the equivalent discrete time channel may be time-varying because the transmitter pulse interval could be different from that of the receiver ($N_rT_r \neq N_tT_t$), and Eq. (4) can not be expressed as the convolution of signal sequences. Generally, N_rT_r and N_tT_t may not divide each other and

$$\frac{N_tT_t}{N_rT_r} = \frac{B_tN_t}{N_r} = \frac{\tilde{N}_t}{\tilde{N}_r}\ , \qquad (5)$$

where $\tilde{N}_t = B_tN_t/\text{gcd}\{B_tN_t, N_r\}$ and $\tilde{N}_r = N_r/\text{gcd}\{B_tN_t, N_r\}$.

With Eq. (5), we can factorize the indices of the transmitted and received samples by $k = m\tilde{N}_t + q$, $q \in [0, \tilde{N}_t - 1]$, $n = g\tilde{N}_r + d$, $d \in [0, \tilde{N}_r - 1]$. Then, we have [c.f. (4)]

$$\begin{aligned}\tilde{x}(m;q) = \sum_{b=0}^{B_t-1}\sum_{d=0}^{\tilde{N}_r-1}\sum_{g=0}^{\infty}\tilde{v}(g;d,b)R_{t,r}\Big(m\tilde{N}_tN_rT_r \\ -g\tilde{N}_rN_tT_t + qN_rT_r - dN_tT_t; b\Big) + \tilde{\eta}(m;q)\ ,\end{aligned} \qquad (6)$$

where $\tilde{x}(m;q) = x(m\tilde{N}_t + q)$, $\tilde{\eta}(m;q) = \eta(m\tilde{N}_t + q)$ and $\tilde{v}(g;d,b) = v(g\tilde{N}_r + d; b)$. Defining $\tilde{h}(l;q,d,b) = R_{t,r}(l\tilde{N}_rN_tT_t + qN_rT_r - dN_tT_t; b)$ as the amplitude of the discrete-time equivalent channel taps, we have the following I/O relationship

$$\begin{aligned}\tilde{x}(m;q) = \sum_{b=0}^{B_t-1}\sum_{d=0}^{\tilde{N}_r-1}\sum_{g=0}^{\infty}\tilde{v}(g;d,b)\tilde{h}\,(m-g;q,d,b) \\ + \tilde{\eta}(m;q)\ ,\ q \in [0, \tilde{N}_t - 1].\end{aligned} \qquad (7)$$

In deriving Eq. (7), we used the relationship $\tilde{N}_tN_rT_r = \tilde{N}_rN_tT_t$. If the (d,b) pair is mapped to a single index p by $p = d + b\tilde{N}_r$, we can rewrite Eq. (7) as

$$\begin{aligned}\tilde{x}(m;q) = \sum_{p=0}^{B_t\tilde{N}_r-1}\sum_{g=0}^{\infty}\tilde{v}(g;p)\tilde{h}\,(m-g;q,p) + \tilde{\eta}(m;q)\ , \\ q \in [0, \tilde{N}_t - 1]\ ,\end{aligned} \qquad (8)$$

where $\tilde{v}(g;p) = \tilde{v}(g;d,b)$ and $\tilde{h}(m-g;q,p) = \tilde{h}(m-g;q,d,b)$.

Eq. (8) indicates that when $B_t\tilde{N}_r$ data streams $\tilde{v}(n;p)$, $p \in [0, B_t\tilde{N}_r - 1]$ are transmitted, $\tilde{N}_t$ data streams $\tilde{x}(n;q)$, $q \in [0, \tilde{N}_t - 1]$ will be received at the receiver. This relationship constitutes a MIMO system with $B_t\tilde{N}_r$ input ports and $\tilde{N}_t$ output ports, which has also been utilized for multiantenna systems. The minimum interval for Eq. (8) to hold is $\tilde{N}_rN_tT_t$, during which only one symbol is transmitted through each subchannel of the equivalent MIMO system. For multiantenna systems, the MIMO model captures the spatial characteristic by deploying multiple Tx- and Rx-antennas. While, for asymmetric UWB links, the MIMO model reflects the transceiver asymmetry due to the different band numbers and different sampling rates. In addition, when the transmitter and the receiver both use a single band, the asymmetric link becomes a multirate system which has been well investigated in the multirate signal processing area (see, e.g., [5]).

There are benefits when we use Eq. (8) to model the asymmetric UWB link. First, although the real channel is time-invariant, the overall discrete time channel $R_{t,r}(\cdot)$ is time-varying, due to the asymmetry between the transmitter and the receiver. However, the equivalent channel for each subchannel remains time-invariant, which makes the subsequent signal processing more convenient. More importantly, after the conversion to the MIMO model, existing system design methods for multiantenna systems can be applied to optimize the asymmetric UWB link in terms of throughput, error performance or complexity (see, e.g., [22], [25], [26], [34]).

Based on the preceding discussions, we have the following result

Proposition 1 *For the asymmetric UWB link consisting of single-antenna transceivers illustrated in Fig. 1, when the transmitter operates with B_t bands and pulse rate of $1/(N_tT_t)$, and the receiver operates with a single band and pulse rate of $1/(N_rT_r)$, the system can be modeled and optimally designed as a MIMO system corresponding to the multiantenna system with $B_t\tilde{N}_r$ Tx-antennas and $\tilde{N}_t$ Rx-antennas, with $\tilde{N}_t = B_tN_t/gcd\{B_tN_t, N_r\}$ and $\tilde{N}_r = N_r/gcd\{B_tN_t, N_r\}$.*

B. Single-Band Transmitter and Multiband Receiver

Next, let us investigate the modeling of the asymmetric UWB link where the transmitter operates with a single band and the receiver captures the received signal over B_r bands. As stated in the preceding section, the receiver can be regarded as another type of the channelized UWB receiver proposed in [7], [20]. Suppose that the pulse rate of the transmitter is

$1/(N_tT_t)$ and the sampling rate at the receiver is $1/(N_rT_r)$, with T_t and T_r being the width of the pulse shapers at the transmitter and receiver, respectively. We choose $T_r = B_rT_t$ such that the transmitter and receiver can access the same bandwidth.

Following the multiband transmitter to single-band receiver case, we can derive the equivalent MIMO system model for the single-band transmitter and multiband receiver link.

Proposition 2 *For the asymmetric UWB link consisting of single-antenna transceivers illustrated in Fig. 1, when the transmitter operates with a single band and pulse rate of $1/(N_tT_t)$, and the receiver operates with B_r bands and pulse rate of $1/(N_rT_r)$, the system can be modeled and optimally designed as a MIMO model corresponding to the multiantenna system with $\tilde{N}_r$ Tx-antennas and $B_r\tilde{N}_t$ Rx-antennas, with $\tilde{N}_t = N_t/gcd\{N_t, B_rN_r\}$ and $\tilde{N}_r = B_rN_r/gcd\{N_t, B_rN_r\}$.*

C. Special Cases

It has been shown that the asymmetric UWB link can be converted to an equivalent MIMO system model. By selecting some special values of the band number, the Tx pulse rate and the Rx pulse rate, we can realize the conversion with simpler models including both the multiple-input and single-output (MISO) and the single-input and multiple-output (SIMO) models. In particular, a MISO system model with M input ports can be realized by setting $B_t = 1$, $B_r = 1$ and $N_t/N_r = 1/M$, and a SIMO system with M output ports can be realized by setting $B_t = 1$, $B_r = 1$ and $N_t/N_r = M$, with M being an integer. If both the transmitter and receiver operate with a single band and the Tx pulse rate is equal to the Rx sample rate, i.e. $T_r = T_t$ and $N_r = N_t$, the UWB link becomes symmetric and can be modeled by the normal single-input and single-output (SISO) model.

IV. Block Transmission

In Eq. (8), the minimum time interval for the MIMO model to hold is $T_s := \tilde{N}_rN_tT_t = \tilde{N}_tN_rT_r$, during which only one symbol is transmitted over each of the equivalent subchannels. Hence, in a block-by-block transmission and processing of information symbols, the block size should be integer multiples of T_s.

A. Multiband Transmitter and Single-Band Receiver

Let us consider the block transmission where during each transmission period, N_s information symbols are transmitted over each subchannel of the equivalent MIMO system. During the nth transmission period $[nN_sT_s, (n+1)N_sT_s)$, the transmitted symbols are $\tilde{\boldsymbol{v}}(n;p) = [\tilde{v}(nN_s;p), \tilde{v}(nN_s + 1;p), \ldots, \tilde{v}((n+1)N_s - 1;p)]^T$, $p \in [0, B_t\tilde{N}_r - 1]$, and the received signals are $\tilde{\boldsymbol{x}}(n;q) = [\tilde{x}(nN_s;q), \tilde{x}(nN_s + 1;q), \ldots, \tilde{x}((n+1)N_s - 1;q)]^T$, $q \in [0, \tilde{N}_t - 1]$. The block transmission can then be expressed in matrix form as [c.f. (8)]

$$\tilde{\boldsymbol{x}}(n;q) = \sum_{p=0}^{B_t\tilde{N}_r-1} \Big[\boldsymbol{H}(q,p)\tilde{\boldsymbol{v}}(n;p) + \breve{\boldsymbol{H}}(q,p) \times \tilde{\boldsymbol{v}}(n-1;p)\Big] + \tilde{\boldsymbol{\eta}}(n;q)\ ,\ q \in [0, \tilde{N}_t - 1]\ , \tag{9}$$

where $\boldsymbol{H}(q,p)$ and $\breve{\boldsymbol{H}}(q,p)$ are $N_s \times N_s$ lower and upper triangular Toeplitz matrices, and $\tilde{\boldsymbol{\eta}}(n;q)$ is the associated noise vector. In Eq. (9), terms inside the square bracket constitute the block-by-block I/O relationship for a single Tx- and Rx-antenna system, with $\tilde{\boldsymbol{v}}(n-1;p)$ reflecting the inter-block-interference (IBI) induced by the channel multipath effect (see, e.g., [32]). With (q,p) varying in the ranges of $q \in [0, \tilde{N}_t - 1]$ and $p \in [0, B_t\tilde{N}_r - 1]$, Eq. (9) represents the MIMO block-by-block I/O model of the asymmetric UWB link, and $\boldsymbol{H}(q,p)$ as well as $\breve{\boldsymbol{H}}(q,p)$ corresponds to the equivalent subchannel between the pth input port and qth output port of the MIMO model.

With the MIMO representation of Eq. (9), we can easily adopt existing multiantenna techniques for the optimal design of the asymmetric UWB link. However, in Eq. (9), neither the transmitted nor the received signal is arranged in the order in which they are transmitted or received. In order to complete the Tx and Rx processing, we need to know the relationship between Eq. (9) and the "real" system I/O relationship given as follows

$$\boldsymbol{x}(n) = \boldsymbol{\mathcal{H}}\boldsymbol{v}(n) + \breve{\boldsymbol{\mathcal{H}}}\boldsymbol{v}(n-1) + \boldsymbol{\eta}(n)\ , \tag{10}$$

where $\boldsymbol{x}(n)$ and $\boldsymbol{v}(n)$ are arranged in the order in which they are transmitted or received; $\boldsymbol{\mathcal{H}}$ and $\breve{\boldsymbol{\mathcal{H}}}$ are two $N_s\tilde{N}_t \times N_sB_t\tilde{N}_r$ channel matrices. We term Eq. (10) as the SISO representation of the asymmetric UWB link consisting of a single Tx-antenna and a single Rx-antenna. Because the discrete time channel in Eq. (4) is time-varying, $\boldsymbol{\mathcal{H}}$ and $\breve{\boldsymbol{\mathcal{H}}}$ are *not* Toeplitz matrices, which is the essential difference between the MIMO representation (9) and the SISO representation (10).

In order to establish the relationship between Eqs. (9) and (10), we first rewrite the MIMO representation Eq. (9) with a single channel matrix of larger dimension. Stacking the transmitted and the received signals into vectors $\tilde{\boldsymbol{v}}(n) = [\tilde{\boldsymbol{v}}^T(n;0), \tilde{\boldsymbol{v}}^T(n;1), \ldots, \tilde{\boldsymbol{v}}^T(n;B_t\tilde{N}_r - 1)]^T$ and $\tilde{\boldsymbol{x}}(n) = [\tilde{\boldsymbol{x}}^T(n;0), \tilde{\boldsymbol{x}}^T(n;1), \ldots, \tilde{\boldsymbol{x}}^T(n;\tilde{N}_t - 1)]^T$, we can rewrite Eq. (9) as

$$\tilde{\boldsymbol{x}}(n) = \boldsymbol{H}\tilde{\boldsymbol{v}}(n) + \breve{\boldsymbol{H}}\tilde{\boldsymbol{v}}(n-1) + \tilde{\boldsymbol{\eta}}(n)\ , \tag{11}$$

where $\tilde{\boldsymbol{\eta}}(n)$ is the noise vector associated with $\tilde{\boldsymbol{x}}(n)$. The channel matrix $\boldsymbol{H}$ collects the channel information of all $\tilde{N}_t \times B_t\tilde{N}_r$ subchannels of the MIMO model as

$$\boldsymbol{H} = \begin{bmatrix} \boldsymbol{H}(0,0) & \boldsymbol{H}(0,1) & \cdots & \boldsymbol{H}(0, B_t\tilde{N}_r - 1) \\ \boldsymbol{H}(1,0) & \boldsymbol{H}(1,1) & \cdots & \boldsymbol{H}(1, B_t\tilde{N}_r - 1) \\ \vdots & \vdots & \ddots & \vdots \\ \boldsymbol{H}(\tilde{N}_t - 1, 0) & \boldsymbol{H}(\tilde{N}_t - 1, 1) & \cdots & \boldsymbol{H}(\tilde{N}_t - 1, B_t\tilde{N}_r - 1) \end{bmatrix}$$

and $\breve{\boldsymbol{H}}$ has the same size and structure as $\boldsymbol{H}$, but with $\boldsymbol{H}(q,p)$ replaced by $\breve{\boldsymbol{H}}(q,p)$, $p \in [0, B_t\tilde{N}_r - 1]$, $q \in [0, \tilde{N}_t - 1]$.

In the Appendix, we will derive the relationship between the MIMO and SISO representations: $\boldsymbol{v}(n) = \boldsymbol{P}_t\tilde{\boldsymbol{v}}(n)$, $\boldsymbol{x}(n) = \boldsymbol{P}_r\tilde{\boldsymbol{x}}(n)$, $\boldsymbol{H} = \boldsymbol{P}_r^T\boldsymbol{\mathcal{H}}\boldsymbol{P}_t$ and $\breve{\boldsymbol{H}} = \boldsymbol{P}_r^T\breve{\boldsymbol{\mathcal{H}}}\boldsymbol{P}_t$, with $\boldsymbol{P}_t$ and $\boldsymbol{P}_r$ being the Tx and Rx permutation matrices, respectively. Examples of $\boldsymbol{\mathcal{H}}$ and $\boldsymbol{H}$ are shown in Fig. 2 and Fig. 3. We notice that after the permutation operation, the equivalent channel matrix $\boldsymbol{\mathcal{H}}$ has a block-wise square and Toeplitz structure.

Combining Eqs. (10) and (11), we have the following result:

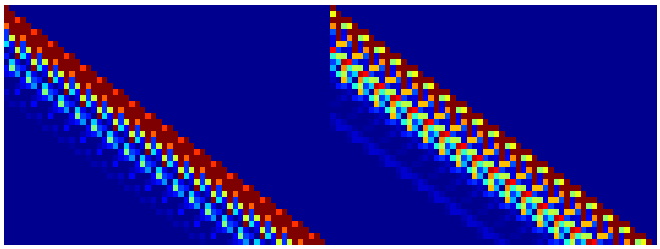

Fig. 2. Example of $\boldsymbol{\mathcal{H}}$ with $\tilde{N}_t = 2$, $\tilde{N}_r = 3$ and $B_t = 2$.

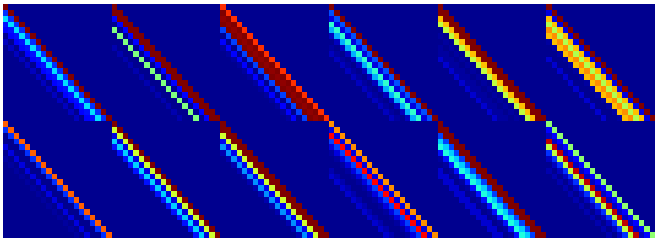

Fig. 3. Example of $\boldsymbol{H}$ with $\tilde{N}_t = 2$, $\tilde{N}_r = 3$ and $B_t = 2$.

Proposition 3 *For the asymmetric UWB link captured by an equivalent $B_t\tilde{N}_r \times \tilde{N}_t$ MIMO model, the channel matrices $\boldsymbol{\mathcal{H}}$ and $\breve{\boldsymbol{\mathcal{H}}}$ can be converted into $(N_s\tilde{N}_t) \times (N_s B_t \tilde{N}_r)$ block-wise Toeplitz matrices as follows:*

$$\boldsymbol{H} = \boldsymbol{P}_r^T \boldsymbol{\mathcal{H}} \boldsymbol{P}_t, \qquad \breve{\boldsymbol{H}} = \boldsymbol{P}_r^T \breve{\boldsymbol{\mathcal{H}}} \boldsymbol{P}_t \,, \tag{12}$$

where the permutation matrices $\boldsymbol{P}_t$ and $\boldsymbol{P}_r$ are defined in the Appendix. The resulting channel matrices $\boldsymbol{\mathcal{H}}$ and $\breve{\boldsymbol{\mathcal{H}}}$ both consist of $B_t\tilde{N}_t\tilde{N}_r$ blocks, with their corresponding (q,p)th blocks being $N_s \times N_s$ lower and upper triangular Toeplitz matrices generated by the subchannel between the pth input port and the qth output port of the MIMO model.

Proposition 3 indicates that, by simply employing two permutation operators at the transmitter and receiver, the time-varying discrete-time channel turns into a MIMO frequency-selective channel with $B_t\tilde{N}_r$ input ports and $\tilde{N}_t$ output ports. It is worth mentioning that the permutation $\boldsymbol{P}_t$ and $\boldsymbol{P}_r^T$ can be easily implemented with interleavers $\pi\{N_s, B_t\tilde{N}_r\}$ and $\pi\{\tilde{N}_t, N_s\}$, respectively.

B. Single-Band Transmitter and Multiband Receiver

For this case, we consider a block transmission during which the number of symbols transmitted through each subchannel is N_s. Following the previous subsection, we can also establish the MIMO and SISO representations as Eqs. (10) and (11) for the asymmetric UWB link composed of the single-band transmitter and the multiband receiver. Similarly, we have the following result:

Proposition 4 *For the asymmetric UWB link captured by an equivalent MIMO system with $\tilde{N}_r$ input ports and $B_r\tilde{N}_t$ output ports, the channel matrices $\boldsymbol{\mathcal{H}}'$ and $\breve{\boldsymbol{\mathcal{H}}}'$ can be converted into $(N_s B_r \tilde{N}_t) \times (N_s \tilde{N}_r)$ block-wise Toeplitz matrices as follows:*

$$\boldsymbol{H}' = \boldsymbol{P}'^T_r \boldsymbol{\mathcal{H}}' \boldsymbol{P}'_t, \qquad \breve{\boldsymbol{H}}' = \boldsymbol{P}'^T_r \breve{\boldsymbol{\mathcal{H}}} \boldsymbol{P}'_t \,, \tag{13}$$

where $\boldsymbol{P}'_t$ and $\boldsymbol{P}'_r$ are the Tx and Rx permutation matrices. The resulting channel matrices $\boldsymbol{H}'$ and $\breve{\boldsymbol{H}}'$ in the MIMO representation both consist of $\tilde{N}_t B_r \tilde{N}_r$ blocks, with their corresponding (q,p)th blocks being $N_s \times N_s$ lower and upper triangular Toeplitz matrices generated by the subchannel between the pth input port and the qth output port of the MIMO model, $p \in [0, \tilde{N}_r - 1]$, $q \in [0, B_r\tilde{N}_t - 1]$. It can be readily proved that $\boldsymbol{P}_t = \boldsymbol{P}_r{}'$, $\boldsymbol{P}_r = \boldsymbol{P}_t{}'$.

V. Equalization and MIMO Signal Processing

In preceding sections, we have seen that the asymmetric UWB link can be represented by a MIMO model. As a result, the time-varying multipath channel can be converted into a group of time-invariant subchannels of the equivalent MIMO system. Therefore, the asymmetric UWB transceiver design problem amounts to the transmission of information through the multipath MIMO channel. Next, we will give an example of integrating existing MIMO techniques for multipath channels into our transceiver design. We will show that the rich multipath diversity in UWB can be harvested in much more flexible ways other than the widely adopted Rake receiver.

Several MIMO communication techniques have been proposed in the multipath channel, such as the generalized delay diversity code (GDD)[10], Lindskog-Paulraj scheme [16] and MIMO with orthogonal frequency division multiplexing (MIMO-OFDM) (see, e.g., [14], [18], [27]), etc. Generally, channel equalizers can be realized in two manners: the time domain equalizer (TDE) such as the maximum-likelihood sequence estimator (MLSE), and the frequency domain equalizer (FDE) including OFDM and the single-carrier frequency domain equalizer (SC-FDE). Same as the SISO system [6], by using the fast Fourier transform (FFT), FDE of MIMO signals [14], [18], [27] can be realized at a complexity much lower than that of TDE [10], [16]. For this reason, in recent years, almost all multipath channel MIMO techniques are based on the OFDM framework.

With OFDM, the multipath channel can be converted into a group of flat fading subchannels each corresponding to an OFDM subcarrier. Then, MIMO technique is independently applied to each subcarrier. There are generally two types of MIMO techniques: space-time coding (STC) which can improve the error performance by exploiting the diversity gain, and the spatial multiplexing that aims at throughput enhancement. In this paper, we will use STC-based MIMO-OFDM as an example of our transceiver design. Its validity can be further verified by comparing the diversity gain with different system parameters via simulations. Note that this diversity is actually due to the multipath effect which is different from the multiantenna diversity exploited by the traditional multiantenna system. Since people are quite familiar with the MIMO-OFDM-based system, we will just briefly introduce how to integrate it into our transceiver design.

A. Multiband Transmitter and Single-Band Receiver

In the nth transmission duration, at the pth input port of the MIMO model, a block of N_c information symbols $\boldsymbol{s}(n;p) = [s_0(n;p),\ s_1(n;p),\ \ldots,\ s_{N_c-1}(n;p)]^T$ are multicarrier modulated on N_c orthogonal digital subcarriers to form $\tilde{\boldsymbol{u}}(n;p) = \boldsymbol{F}^{\mathcal{H}} \boldsymbol{s}(n;p)$, where $\boldsymbol{F}$ is the fast Fourier

TABLE I
MIMO MODEL OF UWB LINK WITH VARYING SYSTEM PARAMETERS

MIMO model	B_t	B_r	T_t(ns)	T_r(ns)	N_t	N_r	Data rate (Mbps)
1×1	1	1	1	1	2	2	400
1×2	1	2	1	2	2	1	400
2×1	2	1	2	1	1	2	400
1×2	1	1	1	1	2	1	400
2×1	1	1	1	1	1	2	400
3×1	3	1	3	1	1	3	266.7
3×2	3	1	3	1	2	3	133.3
3×1	1	1	1	1	1	3	266.7
3×2	1	1	1	1	2	3	133.3

transform (FFT) matrix. By doing that, we actually partition the frequency selective channel into N_c frequency flat fading subchannels. As a result, we have N_c parallel independent MIMO systems each based on one subcarrier.

For each subcarrier $k \in [0,\ N_c-1]$, the symbols $s_k(n;p)$s, $p \in [0, B_t\tilde{N}_r - 1]$ are independently generated by the STC encoder. The $N_g = (N_s - N_c)$ point guard interval (GI) in the form of padding zeros (ZP) or cyclic prefix (CP) is added to each block to mitigate the inter-symbol-interference (ISI). If ZP is adopted, the symbol vector is generated by $\tilde{\boldsymbol{v}}(n;p) = \boldsymbol{T}_{N_s,N_g}\tilde{\boldsymbol{u}}(n;p)$, with $\boldsymbol{T}_{N_s,N_g} = [\boldsymbol{I}_{N_c}, \boldsymbol{0}_{N_c\times N_g}]^T$ being the ZP-inserting matrix. Then, the resulting $\tilde{N}_r \times B_t$ data streams $\tilde{\boldsymbol{v}}(n;p)$s are interleaved and transmitted from the antenna.

At the receiver, remove the GI of the received signal vector at the qth output port of the MIMO model by multiplying $\tilde{\boldsymbol{x}}(n;q)$ with the ZP-wrapping matrix $\boldsymbol{R}_{N_s,N_g} = [\boldsymbol{I}_{N_c}, \boldsymbol{T}_{N_c,N_g}]$. The resulting signal vector is then multicarrier demodulated with FFT operation to generate sequence $\boldsymbol{y}(n;q) = [y_0(n;q), y_1(n;q), \ldots, y_{N_c}(n;q)]^T = \boldsymbol{F}_{N_c}\boldsymbol{R}_{N_s,N_g}\tilde{\boldsymbol{x}}(n;q)$. With some coarse synchronization, it can be easily shown that [c.f. (9)]

$$\boldsymbol{y}(n;q) = \sum_{p=0}^{B_t\tilde{N}_r-1} \sqrt{N_c}\boldsymbol{D}(q,p)\boldsymbol{s}(n;p) + \boldsymbol{\zeta}(n;q)\ , \quad q \in [0, \tilde{N}_t - 1]\ , \tag{14}$$

where $\boldsymbol{D}(q,p)$ is the $N_c \times N_c$ diagonal matrix with the diagonal entries being the FFT coefficients of the discrete-time channel between the pth input port and the qth output port, and $\boldsymbol{\zeta}(n;q)$ is the noise vector. For each subcarrier $k \in [0,\ N_c-1]$, the received signals $y_k(n;q)$s, $q \in [0, \tilde{N}_t - 1]$ are independently STC decoded to obtain the decision statistics.

Stack $\boldsymbol{s}(n;p)$s and $\boldsymbol{y}(n;q)$s into vectors $\boldsymbol{s}(n) = [\boldsymbol{s}^T(n;0), \boldsymbol{s}^T(n;1,0), \ldots, \boldsymbol{s}^T(n;B_t\tilde{N}_r - 1)]^T$ and $\boldsymbol{y}(n) = [\boldsymbol{y}^T(n;0), \boldsymbol{y}^T(n;1), \ldots, \boldsymbol{y}^T(n;\tilde{N}_t - 1)]^T$. Using Proposition 3, we have the Tx and Rx processing for the MIMO-OFDM-based transceiver

$$\begin{aligned} \boldsymbol{v}(n) &= \boldsymbol{P}_t\left(\boldsymbol{I}_{\tilde{N}_r B_t} \otimes \boldsymbol{T}_{N_s,N_g}\right)\left(\boldsymbol{I}_{\tilde{N}_r B_t} \otimes \boldsymbol{F}_{N_c}^{\mathcal{H}}\right)\boldsymbol{s}(n) \\ \boldsymbol{y}(n) &= \left(\boldsymbol{I}_{\tilde{N}_t} \otimes \boldsymbol{F}_{N_c}\right)\left(\boldsymbol{I}_{\tilde{N}_t} \otimes \boldsymbol{R}_{N_s,N_g}\right)\boldsymbol{P}_r^T\boldsymbol{x}(n) \end{aligned}\ . \tag{15}$$

B. Single-Band Transmitter and Multiband Receiver

Similar to the preceding subsection, the MIMO-OFDM transmission can also be realized for the single-band transmitter and multiband receiver link. The required Tx and Rx processing is given by

$$\begin{aligned} \boldsymbol{v}(n) &= \boldsymbol{P'}_t\left(\boldsymbol{I}_{\tilde{N}_r} \otimes \boldsymbol{T}_{N_s,N_g}\right)\left(\boldsymbol{I}_{\tilde{N}_r} \otimes \boldsymbol{F}_{N_c}^{\mathcal{H}}\right)\boldsymbol{s}(n) \\ \boldsymbol{y}(n) &= \left(\boldsymbol{I}_{\tilde{N}_t B_r} \otimes \boldsymbol{F}_{N_c}\right)\left(\boldsymbol{I}_{\tilde{N}_t B_r} \otimes \boldsymbol{R}_{M_e,L_e}\right)\boldsymbol{P'}_r^T\boldsymbol{x}(n) \end{aligned}\ . \tag{16}$$

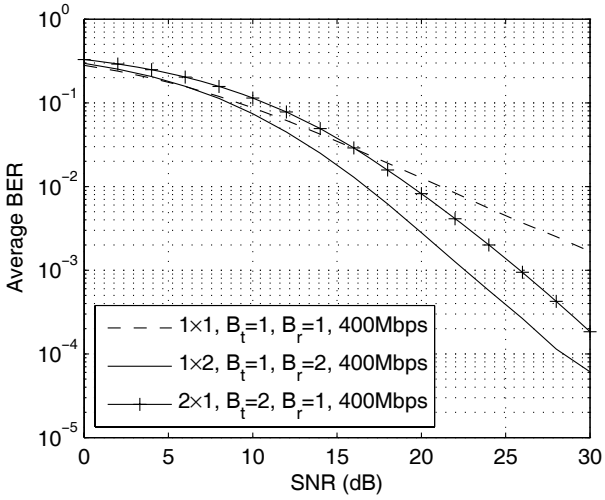

Fig. 4. BER performance for asymmetric UWB links for fixed data rate.

VI. SIMULATIONS

In this section, the transceiver design of asymmetric UWB links will be evaluated via simulations. We use the second-order derivative Gaussian pulse with varying pulse width as the pulse shaper. Simulations are carried out in the IEEE 802.15.3a line-of-sight (LoS) office channel model (CM1) in [8] with a maximum delay spread of about 60ns. In order to avoid the ISI, we use a total of 60ns padding zeros. Length of each signal block is 300ns including ZP. STC techniques are adopted to exploit the diversity which is equal to the product of the input and output port numbers, i.e., the subchannel number of the MIMO system (see, e.g., [13], [29]). It should be noted that the diversity gain exploited here is essentially the channel multipath diversity instead of the multiantenna diversity of the conventional multiantenna system. By altering the system parameters including (B_t, N_t, T_t) and (B_r, N_r, T_r), we can obtain a MIMO system with various structures. All parameter combinations in our simulations together with their corresponding link data rates are shown in table I.

First, we compare the BER performance of different scenarios when the data rate is fixed (see Fig. 4). Alamouti code [2] is adopted for the 2×1 MIMO model and the maximum ratio combining (MRC) is used for the 1×2 one. As a performance benchmark, we also include the BER curve of the SISO model. Given that the duration of each BPSK symbol block is 300ns, all three links can achieve a transmission rate of 400Mbps. Fig. 4 shows that with a larger subchannel number, the equivalent 1×2 SIMO and 2×1 MISO models outperform the SISO one in terms of diversity gain, which is shown by their larger slopes of the BER curves. This subchannel number versus diversity gain relationship has been observed in multiantenna-based MIMO systems (see, e.g., [23]). The SIMO link outperforms the MISO link in terms of coding gain, which is defined as the horizontal shift of the BER curves with the same coding gain.

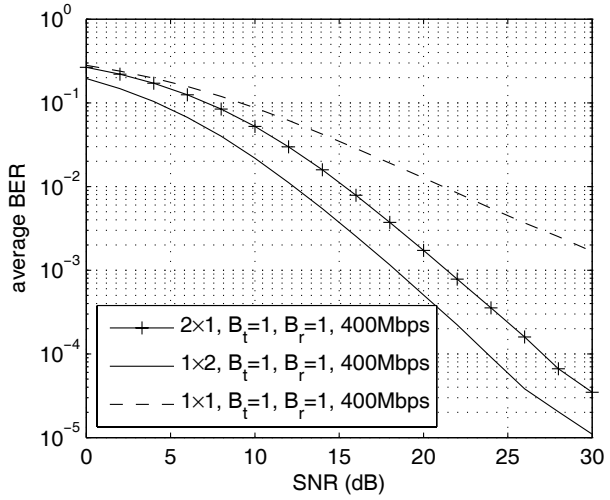

Fig. 5. BER performance for asymmetric UWB links for fixed data rate.

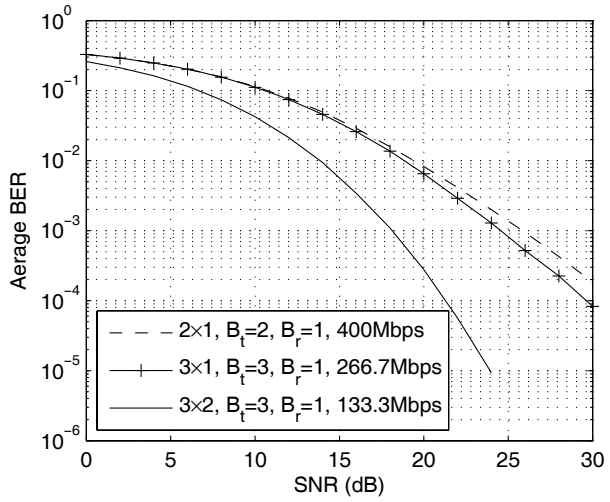

Fig. 6. BER performance for asymmetric UWB links with OSTBC.

This implies that increasing the complexity of the receiver can improve the BER performance, which has been seen in multiantenna systems too (see, e.g., [23]).

In Fig. 5, the same system models are realized as those in Fig. 4 but with a single band at both the transmitter and the receiver. Same as Fig. 4, Alamouti code and MRC are used for the 2×1 and 1×2 systems, respectively. Similar results can be obtained in all three cases. It is interesting to notice that when MIMO model is established by frequency domain asymmetry (Fig. 4), i.e., with different numbers of bands at the transmitter and the receiver, the diversity gain is slightly smaller than that when the MIMO relationship is realized by the unequal pulse rates of single-band transceivers (Fig. 5). This is because for the latter case, subchannels are independent since multipaths of the real channel are independent. However, for the former case, subchannels are correlated because the frequency response of the real channel is correlated in frequency domain. As the subchannel dependency induces diversity loss (see, e.g., [30]), systems in Fig. 5 will outperform those of Fig. 4 in terms of diversity gain.

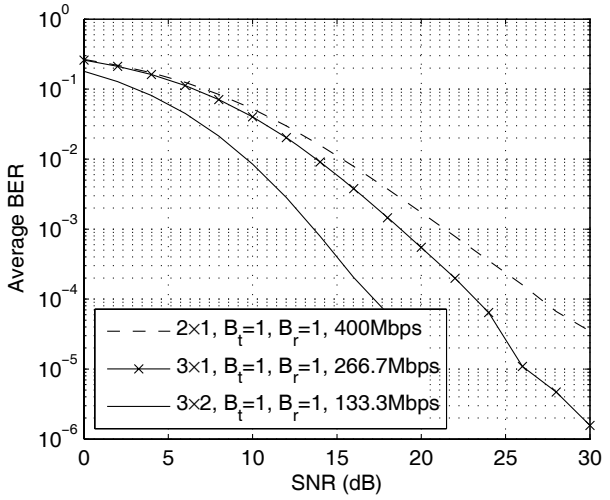

Fig. 7. BER performance for asymmetric UWB links with OSTBC.

In Figs. 6 and 7, we compare the performance of the more general asymmetric UWB links. Orthogonal space-time block codes (OSTBC) are used to exploit the diversity provided by the random channel. OSTBC guarantees that the detection of different symbols can be decoupled, and at the same time the full diversity order can be achieved (see, e.g., [13], [29]) which is equal to subchannel number. From the figures, we can see that the diversity order of the asymmetric link increases as the subchannel number increases. Notice that the data rate decreases as the diversity gain increases. This implies that our transceiver design enables a convenient rate-diversity tradeoff for the single Tx-antenna and single Rx-antenna link. In addition, similar to Figs. 4 and 5, due to the subchannel dependency, the coding gain of the link between a single-band node and a multiband node is lower than that of the link only consisting of single-band nodes.

VII. Conclusions

In this paper, we established the general UWB transceiver model for asymmetric UWB links. It turns out that the asymmetric UWB link can be modeled as a MIMO system, which allows us to exploit the multipath diversity of the single Tx-antenna and single Rx-antenna system in a very flexible manner. Based on these results, we use OFDM-UWB as an example to show how to integrate MIMO signal processing into our transceiver design. Analysis and simulation results confirm that our transceiver design can enable flexible collection of the rich multipath diversity, as well as facilitate convenient rate-diversity tradeoff of the system.

Appendix I: Derivation of Proposition 3

The signal vectors $\boldsymbol{v}(n)$ and $\boldsymbol{x}(n)$ have the same elements as $\tilde{\boldsymbol{v}}(n)$ and $\tilde{\boldsymbol{x}}(n)$ but arranged in a different order. Therefore, $\tilde{\boldsymbol{v}}(n)$ and $\tilde{\boldsymbol{x}}(n)$ can be obtained from $\boldsymbol{v}(n)$ and $\boldsymbol{x}(n)$ using the

$N_s\tilde{N}_rB_t \times N_s\tilde{N}_rB_t$ and $N_s\tilde{N}_t \times N_s\tilde{N}_t$ permutation matrices

$$\boldsymbol{P}_t = \boldsymbol{I}_{B_t} \otimes [\boldsymbol{e}_1, \boldsymbol{e}_{\tilde{N}_r+1}, \ldots, \boldsymbol{e}_{(N_s-1)\tilde{N}_r+1}, \boldsymbol{e}_2, \boldsymbol{e}_{\tilde{N}_r+2}, \ldots, \boldsymbol{e}_{(N_s-1)\tilde{N}_r+2}, \ldots, \boldsymbol{e}_{\tilde{N}_r}, \boldsymbol{e}_{2\tilde{N}_r}, \ldots, \boldsymbol{e}_{N_s\tilde{N}_r}]$$

$$\boldsymbol{P}_r = [\boldsymbol{e}_1, \boldsymbol{e}_{\tilde{N}_t+1}, \ldots, \boldsymbol{e}_{(N_s-1)\tilde{N}_t+1}, \boldsymbol{e}_2, \boldsymbol{e}_{\tilde{N}_t+2}, \ldots, \boldsymbol{e}_{(N_s-1)\tilde{N}_t+2}, \ldots, \boldsymbol{e}_{\tilde{N}_t}, \boldsymbol{e}_{2\tilde{N}_t}, \ldots, \boldsymbol{e}_{N_s\tilde{N}_t}]$$

by

$$\boldsymbol{x}(n) = \boldsymbol{P}_r\tilde{\boldsymbol{x}}(n)\ ,\ \boldsymbol{v}(n) = \boldsymbol{P}_t\tilde{\boldsymbol{v}}(n)\ . \tag{17}$$

These relationships imply that [c.f. (10)] $\boldsymbol{P}_r\tilde{\boldsymbol{x}}(n) = \boldsymbol{\mathcal{H}}\boldsymbol{P}_t\tilde{\boldsymbol{v}}(n) + \breve{\boldsymbol{\mathcal{H}}}\boldsymbol{P}_t\boldsymbol{v}(n-1) + \boldsymbol{\eta}(n)$. As the permutation matrix is orthogonal, we can rewrite this equation as

$$\tilde{\boldsymbol{x}}(n) = \boldsymbol{P}_r^T\boldsymbol{\mathcal{H}}\boldsymbol{P}_t\tilde{\boldsymbol{v}}(n) + \boldsymbol{P}_r^T\breve{\boldsymbol{\mathcal{H}}}\boldsymbol{P}_t\boldsymbol{v}(n-1) + \boldsymbol{P}_r^T\boldsymbol{\eta}(n)\ . \tag{18}$$

Comparing Eq. (18) with the MIMO representation (11), we obtain the relationships of channel matrices between the MIMO and SISO representations as

$$\boldsymbol{H} = \boldsymbol{P}_r^T\boldsymbol{\mathcal{H}}\boldsymbol{P}_t\ ,\ \breve{\boldsymbol{H}} = \boldsymbol{P}_r^T\breve{\boldsymbol{\mathcal{H}}}\boldsymbol{P}_t\ . \tag{19}$$

REFERENCES

[1] "Part 15.4: wireless medium access control (MAC) and physical layer (PHY) specifications for low-rate wireless personal area networks (WPANs), amendment 1: add alternate PHYs," approved Mar. 2007, IEEE-SA Standards Board.

[2] S. M. Alamouti, "A simple transmit diversity technique for wireless communications," *IEEE J. Sel. Areas Commun.*, vol. 16, no. 8, pp. 1451-1458, Oct. 1998.

[3] L. Badia, M. Miozzo, M. Rossi, and M. Zorzi, "Routing schemes in heterogeneous wireless networks based on access advertisement and backward utilities for QoS support," *IEEE Commun. Mag.*, vol. 45, no. 2, pp. 67-73, Feb. 2007.

[4] R. Blazquez, P. P. Newaskar, F. S. Lee, and A. P. Chandrakasan, "A baseband processor for impulse ultra-wideband communications," *IEEE J. Solid-State Circuits*, vol. 40, no. 9, pp. 1821-1828, Sep. 2005.

[5] R. E. Crochiere and L. R. Rabiner, *Multirate Digital Signal Processing*. Prentice Hall, 1996.

[6] D. Falconer, S. L. Ariyavisitakul, A. Benyamin-Seeyar, and B. Eidson, "Frequency domain equalization for single-carrier broadband wireless systems," *IEEE Commun. Mag.*, vol. 40, no. 4, pp. 58-66, Apr. 2002.

[7] L. Feng and W. Namgoong, "An oversampled channelized UWB receiver with transmitted reference modulation," *IEEE Trans. Wireless Commun.*, vol. 5, no. 6, pp. 1497-1505, June 2006.

[8] J. R. Foerster, Channel Modeling Sub-Committee Report Final, IEEE P802.15-02/368r5-SG3a, IEEE P802.15 Working Group for WPAN, Nov. 2002.

[9] J. R. Foerster, E. Green, S. Somayazulu, and D. Leeper, "Ultra-Wideband technology for short or medium range wireless communications," *Intel Technology Journal*, 2nd quarter, 2001. [Online]. Available: http://developer.intel.com/technology/itj/q22001/pdf/art_4.pdf

[10] D. Gore, S. Sandhu, and A. Paulraj, "Delay diversity code for frequency selective channels," *Electron. Lett.*, vol. 37, no. 20, pp. 1230-1231, Sep. 2001.

[11] I. Guvenc and H. Arslan, "Bit error rates of IR-UWB transceiver types at sub-Nyquist sampling rates," in *Proc. Wireless Commun. Netw. Conf.*, Las Vegas, NV, Apr. 2006, pp. 1080-1085.

[12] S. Hoyos, B. M. Sadler, and G. R. Arce, "Broadband multicarrier communication receiver based on analog to digital conversion in the frequency domain," *IEEE Trans. Wireless Commun.*, vol. 5, no. 3, pp. 652-661, Mar. 2006.

[13] E. G. Larsson and P. Stoica, *Space-Time Block Coding for Wireless Communications*. Cambridge, UK: Cambridge University Press, 2003.

[14] V. K. N. Lau and T. Wu, "Optimal transmission and limited feedback design for OFDM/MIMO systems in frequency selective block fading channels," *IEEE Trans. Wireless Commun.*, vol. 6, no. 5, pp. 1569-1573, May 2007.

[15] H.-B. Li, K. Takizawa, B. Zhen, and R. Kohno, "Body area network and its standardization at IEEE 802.15.MBAN," 16th IST Mobile and Wireless Communications Summit 2007, July 2007.

[16] E. Lindskog and A. Paulraj, "A transmit diversity scheme for channels with intersymbol interference," in *Proc. International Conf. Commun.*, vol. 1, New Orleans, June 2000, pp. 307-311.

[17] K. Liu, L. Cai, and X. Shen, "Multi-class utility-based scheduling for UWB networks," *IEEE Trans. Veh. Technol.*, vol. 57, no. 1, Jan. 2008.

[18] Z. Liu, Y. Xin, and G. B. Giannakis, "Space-time-frequency coded OFDM over frequency-selective fading channels," *IEEE Trans. Signal Process.*, vol. 50, no. 10, pp. 2465-2476, Oct. 2002.

[19] C. L. Martret and G. B. Giannakis, "All-digital impulse radio for wireless cellular systems," *IEEE Trans. Commun.*, vol. 50, no. 9, pp. 1440-1450, Sep. 2002.

[20] W. Namgoong, "A channelized digital ultrawideband receiver," *IEEE Trans. Wireless Commun.*, vol. 2, no. 3, pp. 502-510, May 2003.

[21] I. Oppermann, L. Stoica, A. Rabbachin, Z. Shelby, and J. Haapola, "UWB wireless sensor networks: UWEN—a practical example," *IEEE Commun. Mag.*, vol. 42, no. 12, pp. S27-S32, Dec. 2004.

[22] D. P. Palomar, J. M. Cioffi, and M. A. Lagunas, "Joint Tx-Rx beamforming design for multicarrier MIMO channels: a unified framework for convex optimization," *IEEE Trans. Signal Process.*, vol. 51, no. 9, pp. 2381-2401, Sep. 2003.

[23] A. Paulraj, R. Nabar, and D. Gore, *Introduction to Space-Time Wireless Communications*. Cambridge, UK: Cambridge University Press, 2003.

[24] M. Pendergrass, "Time domain supporting text for 802.15.3 alternate physical layer proposal," IEEE P802.15-03/144r1, IEEE P802.15 Working Group for Wireless Personal Area Networks, Mar. 2003.

[25] G. G. Raleigh and J. M. Cioffi, "Spatio-temporal coding for wireless communication," *IEEE Trans. Commun.*, vol. 46, no. 3, pp. 357-366, Mar. 1998.

[26] A. Scaglione, P. Stoica, S. Barbarossa, G. B. Giannakis, and H. Sampath, "Optimal designs for space-time linear precoders and equalizers," *IEEE Trans. Signal Process.*, vol. 50, no. 5, pp. 1051-1064, May 2002.

[27] G. L. Stuber, J. R. Barry, S. W. McLaughlin, Y. Li, M. A. Ingram, and T. G. Pratt, "Broadband MIMO-OFDM wireless communications," in *Proc. IEEE*, vol. 92, no. 2, pp. 271-294, Feb. 2004.

[28] J. Tang, Z. Xu, and B. M. Sadler, "Performance analysis of b-bit digital receivers for TR-UWB systems with inter-pulse interference," *IEEE Trans. Wireless Commun.*, vol. 6, no. 2, pp. 494-505, Feb. 2007.

[29] V. Tarokh, H. Jafarkhani, and A. R. Calderbank, "Space-time block codes from orthogonal designs," *IEEE Trans. Inf. Theory*, vol. 45, no. 5, pp. 1456-1467, July 1999.

[30] V. Tarokh, N. Seshadri, and A. R. Calderbank, "Space-time codes for high data rate wireless communication: performance criterion and code construction," *IEEE Trans. Inf. Theory*, vol. 44, no. 2, pp. 744-765, Mar. 1998.

[31] S. R. Velazquez, T. Q. Nguyen, and S. R. Broadstone, "Design of hybrid filter banks for analog/digital conversion," *IEEE Trans. Signal Process.*, vol. 46, no. 4, pp. 956-967, Apr. 1998.

[32] Z. Wang and G. B. Giannakis, "Wireless multicarrier communications: where Fourier meets Shannon," *IEEE Signal Process. Mag.*, vol. 47, no. 3, pp. 29-48, May 2000.

[33] H. Xu and L. Yang, "Low-complexity transceiver design for asymmetric single/multi-band UWB links," in *Proc. International Conf. Commun.*, Beijing, China, May 2008, pp. 3760-3764.

[34] J. Yang and S. Roy, "On joint transmitter and receiver optimization for multiple-input-multiple-output (MIMO) transmission systems," *IEEE Trans. Commun.*, vol. 42, no. 12, pp. 3221-3231, Dec. 1994.

[35] L. Yang, "Rate-scalable UWB for WPAN with heterogeneous nodes," in *Proc. Intl. Conf. Acoustics, Speech, Signal Process.*, Philadelphia, PA, Mar. 2005, pp. 625-628.

[36] Y. Zhang, W. Liu, Y. Fang, and D. Wu, "Secure localization and authentication in ultra-wideband sensor networks," *IEEE J. Sel. Areas Commun.*, vol. 24, no. 4, pp. 829-835, Apr. 2006.

[37] Z. Zhang, M. Ma, and Y. Yang, "Energy-efficient multihop polling in clusters of two-layered heterogeneous sensor networks," *IEEE Trans. Computers*, vol. 57, no. 2, pp. 231-245, Feb. 2008.

Huilin Xu received the B.Sc. and M. Sc. degrees from the University of Science and Technology of China (USTC), Hefei, China, in 2002 and 2005, respectively, both in Electrical Engineering. He is currently pursuing the Ph.D degree with the Department of Electrical and Computer Engineering, University of Florida, Gainesville, Florida. His research interests are in the areas of wireless communications and related fields.

Liuqing Yang (S'02-M'04-SM'06) received her M.Sc. and Ph.D. degrees in Electrical and Computer Engineering from the University of Minnesota, Minneapolis, in 2002 and 2004, respectively. Since August 2004, she has been with the Department of Electrical and Computer Engineering at the University of Florida, Gainesville, where she is now an Associate Professor. Her current research interests include signal processing, communications theory and networking.

Dr. Yang received the Best Dissertation Award in the Physical Sciences & Engineering from the University of Minnesota in 2005, the Office of Naval Research Young Investigator Award in 2007, and the National Science Foundation Faculty Early Career Development Award in 2009. She is an Associate Editor of the IEEE TRANSACTIONS ON COMMUNICATIONS, IEEE TRANSACTIONS ON WIRELESS COMMUNICATIONS and the IEEE TRANSACTIONS ON INTELLIGENT TRANSPORTATION SYSTEMS. She is also a member of the Editorial Board of PHYCOM: PHYSICAL COMMUNICATIONS. Dr. Yang is presently the vice chair of the IEEE Section of Gainesville, FL, and a co-chair of IEEE Intelligent Transportation Systems Society technical committee on Mobile Communication Networks.